JCTC Journal of Chemical Theory and Computation

The Origin of Layer Structure Artifacts in Simulations of Liquid Water

David van der Spoel* and Paul J. van Maaren

Department of Cell and Molecular Biology, Uppsala University, Husargatan 3, Box 596, SE-751 24 Uppsala, Sweden

Received September 9, 2005

Abstract: A recent paper (Yonetani, *Chem. Phys. Lett.* **2005**, *406*, 49−53) shows that in computer simulations of TIP3P water (Jorgensen et al. *J. Chem. Phys.* **1983**, *79*, 926−935) a strange layer formation can occur when a long cutoff is used. This result is counterintuitive because, in principle, increasing the cutoff should give more accurate results. Here we test this finding for different water models and try to explain why layer formation occurs. In doing so we find that under certain conditions, layer formation coincides with a sharp density increase to 1050 g/L, while simultaneously a pressure of 600 bar develops and water diffusion becomes anisotropic. This leads us to conclude that a group-based cutoff (of at least 1.4 nm) stabilizes an anomalous phase with most water models. In some cases the ordering is strengthened further by periodicity in the simulation cell, but periodicity effects can even be observed with a short cutoff (0.9 nm) and a relatively large box of 4 nm. Water models that have a relatively large quadrupole moment, more in accord with the experimental gas-phase values, in particular TIP4P (Jorgensen et al. *J. Chem. Phys.* **1983**, *79*, 926−935), are much less affected by the problem, because the dipole−dipole interaction is quenched at long distance. A comparison of different cutoff treatments, namely truncation, reaction field, particle mesh Ewald (PME), and switch and shift functions, for the simulation of water shows that only PME and shift functions yield realistic dipole−dipole interactions at long distance. The impact for biomolecular simulations is discussed.

1. Introduction

In a recent paper, Yonetani[1] reported a strange artifact: when TIP3P water[2] is simulated with group-based truncation and a cutoff of 1.8 nm it forms liquid layers in which the molecular dipoles are mainly oriented in the same direction.[1] The artifact was reproduced in two different MD packages, Amber[3] and GROMACS,[4−6] implying that it is not due to a software bug. The layers were also found in larger boxes,[1] indicating that the behavior is a truncation problem rather than being related to the use of periodic boundary conditions. Interestingly, the layer formation does not occur in conjunction with the particle-mesh Ewald (PME)[7,8] method for computing electrostatic interactions. PME is one of the most popular implementations of the Ewald technique, because it is efficient and fast. The electrostatic energy is split into two parts, the short range is computed in direct space and the long range in reciprocal space, using fast Fourier transforms. Other algorithms in practical use for the computation of long-range Coulomb interactions are the particle−particle particle-mesh method,[9,10] fast multipole methods,[11,12] and Lekner summation.[13−16]

Here we present a series of simulations, using different water models and simulation conditions, in an attempt to explain the phenomenon. For a particular set of parameters we find that TIP3P water transforms to a state with a density of 1050 g/L, a pressure of 600 bar, and a potential energy lowered by 1 kJ/mol compared to the normal −40.8 kJ/mol.[17] Similar results are obtained for TIP5P, SPC/E, and SPC water. The simultaneous increase in density and pressure is driven by an increased number of hydrogen bonds and a clearly different, layered, structure; in addition diffusion

* Corresponding author phone: 46-18-4714205; fax: 46-18-511755; e-mail: spoel@xray.bmc.uu.se.

10.1021/ct0502256 CCC: $33.50
Published on Web 11/25/2005

becomes anisotropic. The combination of these observations leads to the conclusion that this is an artificial phase of liquid water.

Complex phenomena such as phase transitions are particularly sensitive to the correctness of the simulation conditions. Slovak and Tanaka have shown[18] in simulation studies of melting of ice VII that with a short (0.8655 nm) "smoothly" truncated potential the melting temperatures are very different from those obtained with Ewald summation. In other studies of phase transitions Zangi and Mark[19] used a twin-range cutoff with reaction field for the Coulomb interaction, while Matsumoto et al.[20] used a shifted potential as first described by Ohmine et al.[21] (Appendix B). From a personal communication we learned that Yamada et al.[22] used a plain cutoff of 0.9 nm (group-based truncation[23,24]), whereas Koga et al.[25] used a cutoff of 0.875 nm with a switching function. Since there is such a plethora of methods for cutoff treatment, it is very important that authors document their work sufficiently[26,27] to allow others to verify it. This work focuses on the treatment of electrostatic interactions, but in principle the accuracy of other simulation algorithms, like integrators and constraint treatment, need to be considered as well. The impact of those algorithms on accuracy fall outside the scope of this paper, however.

2. Methods

Molecular dynamics simulations were performed using the TIP3P and TIP4P water models,[2] the TIP5P model,[28] the SPC model,[29] and the SPC/E model.[30] Berendsen temperature coupling (298.15 K) and pressure coupling (1 bar) were used.[31] The temperature coupling constant τ_T was 0.1 ps, and the pressure coupling constant τ_P was 0.2 ps unless otherwise stated. A compressibility of 0.00005 (1/bar) was used. Although we realize that τ_P is unusually short, we used this value to be compatible with Yonetani;[1] in addition, we explicitly tested the influence of τ_P as described in the results. In all cases a cutoff was used for the Lennard-Jones interactions, but long-range corrections to the energy were applied in the standard way.[23] Neighborlists were used and updated every fifth integration time step, which was 2 fs. The water molecules were kept rigid using the SETTLE algorithm.[32] Center of mass motion of the simulation box was removed at every time step.[33]

Five different cutoff schemes were used: 1. a group-based cutoff (simple truncation at the indicated cutoff distance), 2. a reaction field[34−36] with $\epsilon_{rf} = 78.5$ (Appendix A), 3. the particle-mesh Ewald algorithm,[7,8] 4. an atom-based switch function, and 5. an atom-based shift function (Appendix B). For all simulations molecule-based neighbor searching was done, and for both the cutoff and reaction field it should be noted that the cutoff was based on molecules as well, to avoid artifacts due to non-neutral groups. The atom-based switch and shift functions go to zero smoothly; however, it is known that atom based switch functions can cause artifacts when the switching range is too short.[24] When using PME the grid-spacing was 0.12 nm (fluctuating slightly due to pressure coupling), and fourth-order B-splines were used for charge spreading and force interpolation. Conducting boundary conditions were used for PME.

Table 1. Properties of the Water Molecules Used: Dipole μ, the Components of the Quadrupole Tensor Θ, the Root Mean Square Deviation of the Quadrupole Tensor Elements from the Experimental Values

model	μ (D)	Θ_{xx} (10^{-1}D nm)	Θ_{yy} (10^{-1}D nm)	Θ_{zz} (10^{-1}D nm)	RMSD(Θ) (10^{-1}D nm)
expt	1.855	−2.50	2.63	−0.13	
TIP3P	2.35	−1.68	1.76	−0.08	1.20
TIP4P	2.18	−2.09	2.20	−0.11	0.59
TIP5P	2.29	−1.48	1.65	−0.17	1.42
SPC	2.274	−1.82	2.11	−0.29	0.87
SPC/E	2.351	−1.88	2.19	−0.30	0.78

An overview of the simulations performed and the conditions is given in Table 2. All simulations were 2 ns long unless otherwise stated. In total well over 100 simulations were performed, all using the GROMACS software.[4−6] All simulations used single-precision arithmetic, except one, which was performed in order to check the effect of precision.

3. Results

3.1. Dipole−Dipole Correlation. Analysis of the simulations focuses on dipole orientation; in particular, we look at the distance dependent Kirkwood factor $G_k(r)$[36] according to

$$G_k(r) = \sum_{r_{ij}<r} \frac{\mu_i \cdot \mu_j}{\mu^2} \tag{1}$$

where μ_i and μ_j are the dipole vectors of water molecules i and j, respectively, r_{ij} is the distance between oxygen atoms, and the dielectric constant $\epsilon(0)$ is determined from the fluctuations of the total system dipole.[37]

In Figure 1a we have plotted the cutoff dependence of $G_k(r)$ for TIP3P. Obviously there is a severe artifact around the cutoff distance. This is a well-known problem that has been described in detail before.[17,38] In Figure 1b the average cosine $\langle\cos\rangle$ of the angle between two molecular dipoles at a distance r is given. Here we can clearly see that there is a dip in the function corresponding to an anticorrelation on average around the cutoff distance. Obviously, the orientational correlation between water molecules should approach zero with increasing distance,[39,40] so this is an artifact due to the cutoff. In a further series of simulation of 10 648 TIP3P molecules we varied the cutoff r_c from 0.9 to 3.35 nm. The minimum of the $G_k(r)$ function becomes deeper with increasing r_c, indicating that ever stronger ordering is induced (Figure 1c). This shows that there is nothing special about the cutoff of 1.8 nm that was used by Yonetani.[1] In Figure 1d,e we have plotted the first minimum of the oxygen−oxygen and oxygen−hydrogen radial distribution function (RDF), respectively, for different cutoffs. These parts of the RDF were plotted as it is here that the main difference is visible. The minimum in oxygen−oxygen RDF is slightly less deep with long cutoffs, while it is the reverse for the oxygen hydrogen RDF. Apparently the water structure changes slightly upon increasing the cutoff, to accommodate the higher density (Figure 2).

Table 2. Overview of the Simulations Performed[a]

model(s)	N_{mol}	r_c (nm)	elect.	comment
TIP3P	820	0.9−1.4	cut	0.1 nm increments
TIP3P	2201	0.9−1.8	cut	0.1 nm increments
TIP3P	2201	1.8	cut	double precision
TIP3P	10648	0.9−3.3	twin	rc = 0.9 nm, in 0.1 nm increments
TIP3P	10648	3.05−3.35	twin	rc = 0.9 nm, in 0.1 nm increments
TIP3P SPC SPC/E	1728	0.9−1.8	cut	0.1 nm increments (1 ns)
TIP3P	17608	1.8	cut	
TIP3P	59427	1.8	cut	180 ps only
TIP3P	2201	1.8	cut	$\tau_P = 0$ (i.e. NVT), 0.5, 1.0, and 2.0 ps
TIP3P		1.8	cut	N_{mol} = 1728, 2197, 2744, 3375, 4096, 4913, 5832, 6859, 8000, 9261, 10648, 12167, 13824, 15625, 17576, 19683, 21952
TIP3P	2201	1.8	cut	Anisotropic pressure scaling with $\tau_P = 5$ ps. The box edges were allowed to vary independently.
TIP3P	2201	1.8	cut	Anisotropic pressure scaling with $\tau_P = 5$ ps. Only one of the box edges was allowed to vary, while the others were kept at their initial value of 4.06 nm.
TIP3P	2201	1.8	cut	dodecahedron box
All	2201	1.8	cut	
All	2201	1.8	RF	reaction field[34−36] with $\epsilon_{rf} = 78.5$
SPC SPC/E	2201	1.8	RF	reaction field with $\epsilon_{rf} = \infty$ and with the so-called "self-consistent" $\epsilon_{rf} = 54$ (SPC) and 62.3 (SPC/E) as determined by Smith and Van Gunsteren[38] as well as additional simulations with $\epsilon_{rf} = 65$ (SPC) and 77 (SPC/E).
All	2201	0.9	PME	particle-mesh Ewald method[7, 8]
All	2201	1.7	switch	switch function (see Appendix) with a cutoff of 1.7 nm, a 0.2 nm switching range (i.e. $r_1 = 1.5$, $r_c = 1.7$ nm), neighborlists were computed with a 1.8 nm cutoff
All	2201	1.7	switch	switch function (see Appendix) with a cutoff of 1.7 nm, a 0.4 nm switching range (i.e. $r_1 = 1.3$, $r_c = 1.7$ nm), neighborlists were computed with a 1.8 nm cutoff
All	2201	1.7	shift	shift function with a cutoff r_c of 1.7 nm, neighborlists were computed with a 1.8 nm cutoff
TIP3P	17608	0.9	PME	
TIP3P	2201	0.9	PME	dodecahedron box

[a] Water model, number of molecules, cutoff distance, and electrostatics treatment. "All" in column model indicates, TIP3P, TIP4P, TIP5P, SPC, and SPC/E.

The energy (Figure 2a) and density (Figure 2b) show a weird cutoff dependence, which is related to layer formation. For instance for $r_c = 1.5$ and 1.7 nm we obtain relatively large error bars (probably) due to intermittent layer formation. Figure 2c shows the dependence of the diffusion constant on the cutoff. Obviously, cutoffs of 1.4 nm and larger induce significant changes in water properties. In Figure 2d we plot the ratio of diffusion coefficients in a plane normal to the box axes and parallel to the box axis. For isotropic diffusion the ratio should be 1. Since the numbers are averaged over the whole simulation, further compensation effects are expected, but for $r_c = 1.7$ nm we see a very strong peak, which hence indicates that relatively stable layers should be present in the simulation. For the anisotropic simulation (described in more detail below) where we have stable layers perpendicular to the *X*-axis, we see that the ratio of diffusion coefficients perpendicular to and along the *X*-axis is less than one, meaning that the diffusion perpendicular to the layer structure is considerably faster than within the layer.

In the extensive series of simulations that we have performed, we found that in some cases the artifacts get even worse. In a particular case, when anisotropic pressure scaling was used in which only a single axis of the simulation box was allowed to fluctuate, very stable layer formation occurred. Figure 3 shows how several properties evolve in a simulation of 2201 TIP3P molecules under these conditions. Figure 3a shows how the average pressure suddenly increases to 600 bar after roughly 616 ps, while simultaneously the density increases to 1050 g/L (Figure 3b) and the energy drops by 1 kJ/mol (Figure 3c), due to an additional 0.03 hydrogen bonds per molecule (Figure 3f). Indeed we find that the pressure in the direction of the piston (X) is roughly 1, but in the other two directions it is 600−800. In a normal fluid the pressure in the Y and Z would be released through the X dimension, but not in the case when specific ordering is present (like in this artificial case or e.g. in bilayers). To quantify the occurrence of layers we computed the absolute average orientation of the water molecules with respect to the box axes *i*, and from these we computed the mean square deviation from the isotropic value of 0.5[1]

$$\xi = \sum_{i \in x, y, z} \left(\left| \left\langle \frac{\mu_i}{\mu} \right\rangle \right| - 0.5 \right)^2 \qquad (2)$$

where averaging is over all molecules in the computational box. Figure 3d shows ξ as a function of time. Obviously, a gross-net ordering happens simultaneously with the other events, leading to the conclusion that the whole process can be considered to be a liquid−liquid phase transition. Finally, we found that the mobility increases in the new ordered liquid phase. Since we had suspected that some kind of room-temperature freezing was behind the drastic changes of the water properties, we were surprised to see that the diffusion constant actually increases from 7.3 to 9.7 10^5 cm^2 s^{-1}

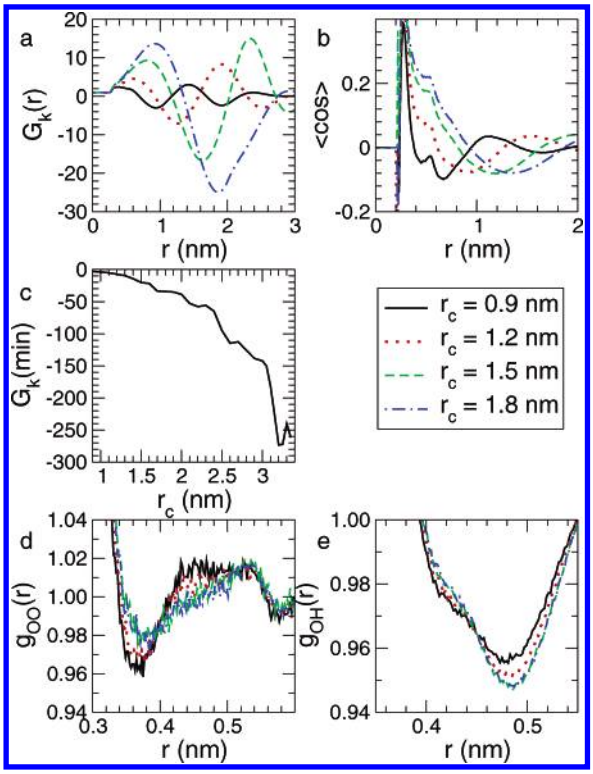

Figure 1. a: The $G_k(r)$ function as a function of the cutoff distance in a TIP3P simulation of 2201 molecules (cutoff r_c indicated in legend), b: ⟨cos⟩ as a function of cutoff in the same set of simulations, c: the depth of the minimum in $G_k(r)$ as a function of cutoff in a series of simulations of 10 648 TIP3P molecules, d: the first minimum in the oxygen−oxygen radial distribution function, and e: the first minimum in the oxygen−hydrogen radial distribution function.

(whereas it is 5.4 for a cutoff of 1.2 nm[17]). On the other hand the increase of diffusion with density and pressure is one of the well-known anomalies of water,[41] and henceforth the high pressure can induce the increased mobility. The artificial water phase can therefore be described as a high-density, high-pressure ordered liquid. There is no special reason anisotropic pressure scaling would facilitate layer formation, other than that in this specific case the width of the box fit the requirement (explained in section 3.4) of being close to an integer times the cutoff.

In Figure 3 we also show what happens when the layered structure is simulated with a short ($r_c = 0.9$ nm) group-based cutoff (from 2000 to 3000 ps). All values fall back quickly to the normal values, showing that layer formation is completely reversible.

3.2. Water Model and Electrostatics Treatment Dependence. To track down how these strange results depend on cutoff treatment and water model, further simulations were performed using the TIP3P and TIP4P models,[2] the TIP5P model,[28] the SPC model,[29] and the SPC/E model.[30] In Figure 4a,f we have plotted again the $G_k(r)$ and the ⟨cos⟩ of the simulations with a 1.8 nm cutoff of the five models. Similarly we have plotted the results from corresponding sets of simulations using a reaction-field (Figure 4b,g), using the PME method (Figure 4c,h), using a switch function (Figure 4d,i), and using a shift function (Figure 4e,j).

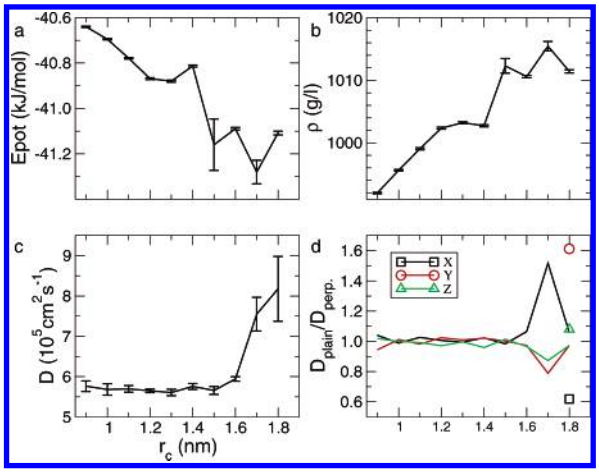

Figure 2. Properties as a function of cutoff in a TIP3P simulation of 2201 molecules using group-based truncation. a: Potential energy, b: density, c: diffusion constant determined by breaking the trajectories in 10 equal pieces of 200 ps, computing the diffusion constant for each molecule separately using the Einstein relation,[23] and taking the average value and standard deviation, and d: ratio of diffusion coefficients in the plane normal to one of the box vectors and along the box vector (for isotropic diffusion the ratio should be 1). The symbols are from the second part of the simulation with anisotropic scaling, i.e., where stable layers are present. Error bars in a and b were determined by a block-averaging procedure.[49]

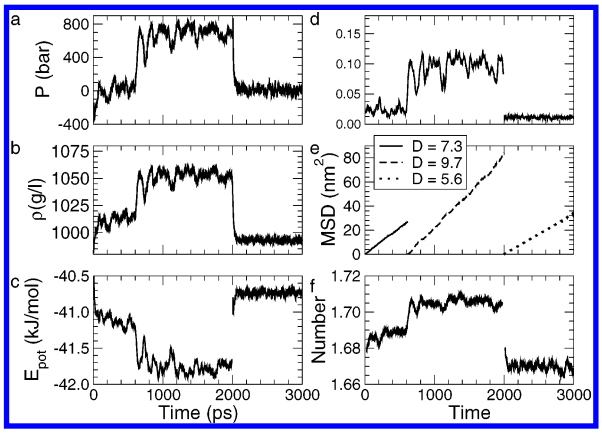

Figure 3. Results from a TIP3P simulation of 2201 molecules where one of the box edges (X) was allowed to fluctuate, while the others were fixed at their initial value of 4.06 nm. The first 2 ns were done with a 1.8 nm cutoff, the third ns was done with a 0.9 nm cutoff, to test reversibility of layer formation. a: Pressure (*bar*), b: density, c: potential energy (kJ/mol), d: ξ (eq 2) and e: mean square displacement computed for three stretches of the trajectory, from 0 to 616 ps (before the phase transition), from 616 to 2000 ps (after), from 2000 to 3000 ps (short cutoff). The resulting diffusion constants (10^5 cm^2 s^{-1}) are indicated, f: the number of hydrogen bonds per molecule. In panels a, c, d, and f a running average over 20 ps is given for clarity.

A number of observations can be made from Figure 4. First, the depression in the $G_k(r)$ function due to the cutoff depends very much on the water model used, but all models are seriously affected. The minimum in Figure 4a is deepest for TIP5P, followed by TIP3P, SPC/E, SPC, and TIP4P.

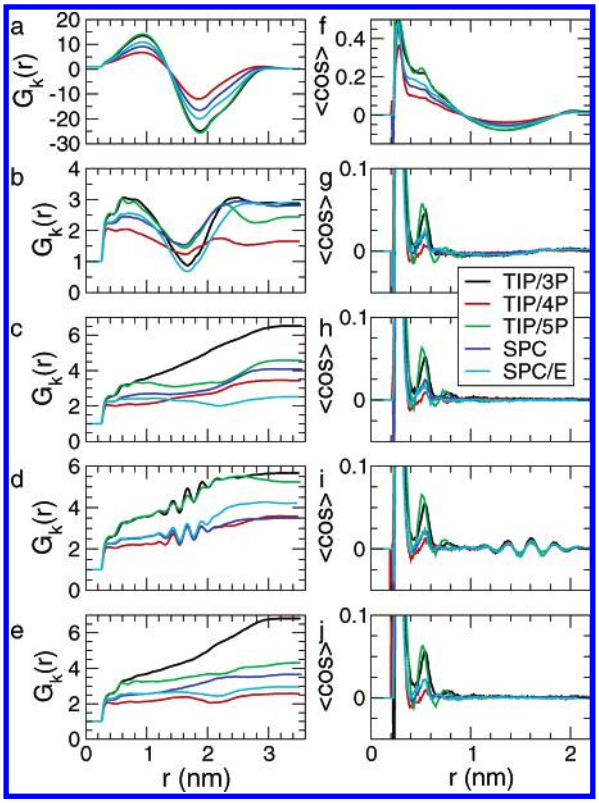

Figure 4. The $G_k(r)$ function for different water models in a cubic box containing 2201 molecules. a: Simulated with 1.8 nm cutoff b: simulated with a reaction field with $\epsilon_{rf} = 78.5$ and a 1.8 nm cutoff, c: simulated with the particle-mesh Ewald technique with a cutoff of 0.9 nm, d: simulated with a switch function and a cutoff of 1.7 nm, and e: simulated with a shift function. The average cosine ⟨cos⟩ of the angle between the dipoles of molecules in a spherical shell at a distance r from a central molecule for f: cutoff, g: reaction-field, h: PME, i: switch function, and j: shift function. Data corresponding to this figure are available as Supporting Information.

Although one would expect the molecular dipole to be decisive about the amount of long-range correlation, in fact we find that SPC/E is much less affected than TIP3P despite having nearly the same dipole, while simultaneously SPC is much less affected than TIP5P. There seems to be a correlation between the depth of the minimum and the magnitude of the molecular quadrupole (Table 1), the only exception being the SPC/E model that is slightly worse than SPC despite having a larger quadrupole. Note that we compare the model quadrupoles (Table 1) to the experimental gas-phase value[42] which need not be the same as the (unknown) liquid-state value.

Second, only the particle-mesh Ewald and the shift function seem to give dependable results that are not affected by the particular choice of cutoff. The shift function, which is a special case of the switch function,[43] seems to alleviate the effects of the cutoff in an efficient way although it obviously will only work correctly when the "real" interaction is zero, i.e., the shift distance should be at least as long as the particular interaction range, which, for water has been estimated to be 1.4−1.5 nm.[39,40] Obviously, ionic interactions cannot be handled faithfully by a shift function. The reason the atom-based switch function gives strange ripples near the cutoff is due to the short switching range which was only 0.2 nm, although this value is commonly used in conjunction with cutoffs in the range of 0.8−1.2 nm. The ripples are reduced somewhat when a longer switching range of 0.4 nm was used (not shown). The alternative of a group-based switch function (Appendix B) is due to the arbitrariness of the group-center definition not attractive in principle, although it probably is devoid of the artifacts (ripples, reduced mobility) we find here. In an attempt to force layer formation using different cutoff treatment, we used anisotropic pressure scaling with 2201 TIP3P molecules. However layering occurred only in combination with the cutoff (Figure 3) and not with any of the other schemes (data not shown).

A list of important observables from the simulations using different cutoff schemes and water models is given in Table 3. The densities are relatively low due to the fact that we did not use the dispersion correction to the pressure (e.g. Wensink et al. find a density of 994 g/L for TIP4P,[44] while

Table 3. Simulation Results from Simulations of 2201 Molecules Using Five Water Models with Six Different Cutoff Schemes, Corresponding to Figure 4: Cutoff and Reaction Field (RF) Simulations with 1.8 nm Cutoff, Particle-Mesh Ewald (PME) with 0.9 nm Cutoff, Switch and Shift with 1.7 nm Cutoff, and Switch with a 0.2 nm Switching Range (See Methods)[a]

model	cutoff	$D\,10^5$ cm^2 s^{-1}	ϵ_0	ρ (g/L)	E_{pot} (kJ/mol)
expt		2.3	78.5	997	−41.7
ref		66, 67	68	69	70
	cutoff	8.2(0.8)	39(1)	1011.4(0.3)	−41.107(0.008)
	RF	5.96(0.06)	94(3)	982.2(0.2)	−39.968(0.002)
TIP3P	PME	5.76(0.03)	92(4)	970.9(0.2)	−39.882(0.002)
	switch	4.26(0.11)	102(5)	1004.3(0.2)	−40.705(0.003)
	Switch2	5.65(0.15)	103(5)	987.3(0.2)	−40.133(0.002)
	Shift	5.8(0.2)	101(5)	981.5(0.2)	−39.823(0.002)
	Cut-Off	3.88(0.02)	48(1)	1000.8(0.2)	−41.698(0.003)
	RF	3.72(0.02)	54(3)	991.0(0.3)	−41.318(0.003)
TIP4P	PME	3.73(0.02)	49(2)	980.4(0.2)	−41.282(0.002)
	switch	2.65(0.02)	53(2)	1026.5(0.2)	−42.293(0.003)
	switch2	3.53(0.08)	52(2)	998.4(0.2)	−41.528(0.003)
	shift	3.78(0.04)	51(2)	990.3(0.2)	−41.172(0.003)
	cutoff	3.9(0.5)	41(1)	1010.9(0.3)	−41.19(0.01)
	RF	3.02(0.03)	72(3)	981.2(0.2)	−40.282(0.005)
TIP5P	PME	2.95(0.05)	88(7)	969.3(0.2)	−40.232(0.006)
	switch	2.72(0.04)	87(6)	988.6(0.3)	−40.353(0.005)
	switch2	2.75(0.07)	89(6)	983.5(0.3)	−40.521(0.005)
	shift	2.94(0.06)	89(6)	980.4(0.2)	−40.139(0.005)
	cutoff	4.48(0.09)	43(1)	991.2(0.2)	−42.359(0.006)
	RF	4.38(0.05)	65(3)	974.3(0.2)	−41.610(0.003)
SPC	PME	4.29(0.04)	67(3)	963.9(0.2)	−41.535(0.003)
	switch	3.24(0.01)	72(4)	1005.5(0.3)	−42.375(0.006)
	switch2	4.11(0.06)	69(3)	982.3(0.2)	−41.794(0.003)
	shift	4.27(0.11)	62(3)	973.9(0.2)	−41.452(0.003)
	cutoff	2.9(0.2)	43(1)	1014.5(0.3)	−47.55(0.01)
	RF	2.71(0.04)	77(4)	996.0(0.2)	−46.668(0.004)
SPC/E	PME	2.70(0.04)	62(4)	986.5(0.2)	−46.618(0.004)
	switch	2.11(0.02)	74(5)	1027.8(0.3)	−47.414(0.005)
	switch2	2.55(0.01)	76(5)	1003.6(0.2)	−46.873(0.004)
	shift	2.71(0.13)	78(5)	995.7(0.2)	−46.515(0.009)

[a] The error in the dielectric constant was determined by computing the error in the square total dipole moment M^2 of the box using a block averaging procedure[65] and multiplying the relative error in M^2 by the dielectric constant.

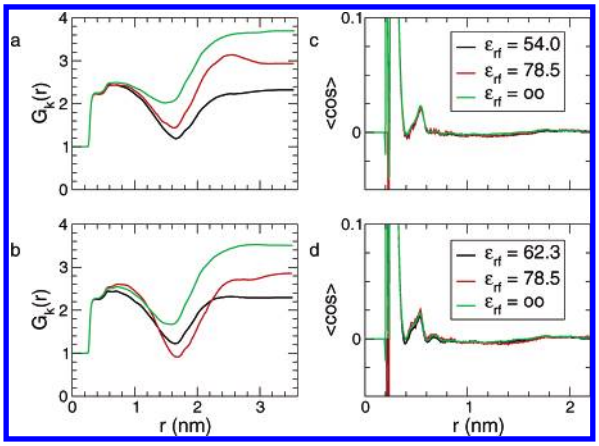

Figure 5. The $G_k(r)$ function for the a: SPC and b: SPC/E water models in a cubic box containing 2201 molecules, simulated with a reaction field with 1.8 nm cutoff and different ϵ_{rf}. The average cosine $\langle\cos\rangle$ of the angle between the dipoles of molecules in a spherical shell at a distance r from a central molecule for c: SPC and d: SPC/E water, under the same conditions as a and b, respectively. Data corresponding to this figure are available as Supporting Information.

Horn et al. find roughly 988 g/L when using explicit tail corrections to a switched Lennard-Jones potential[45]).

3.3. Effect of Reaction Field Parameters. A comparison highlighting the impact of different ϵ_{rf} when using a reaction-field is given in Figure 5. Smith and Van Gunsteren proposed that it would be better to use a ϵ_{rf} close to the dielectric constant of the simulated liquid.[38] They gave reference values for $\epsilon_{rf} = 54$ for SPC and $\epsilon_{rf} = 62.3$ for SPC/E water. Unfortunately the so-called "self-consistent" ϵ_{rf} are dependent on the cutoff as well, and here we find (Table 3) dielectric constants of 65 (SPC) and 77 (SPC/E). Simulation with both values of the dielectric constant were done for each of the two models. The effect of ϵ_{rf} on the potential is a shift of the minimum of the potential. For $\epsilon_{rf} = \infty$ (conducting boundary conditions), the potential has its minimum exactly at the cutoff, for finite ϵ_{rf} the minimum is shifted to (slightly) larger distances. For $\epsilon_{rf} = \infty$ the minimum in $G_k(r)$ is less pronounced than for finite ϵ_{rf} (Figure 5). The self-consistent values are very comparable to the other values that are not self-consistent; however, all of these affect the $G_k(r)$ function considerably more than $\epsilon_{rf} = \infty$ which hence seems to be the best choice for simulations of water. The dielectric constants computed from the different simulation as well as the depth of the minima in the $G_k(r)$ function are given in Table 4. We conclude that use of the self-consistent ϵ_{rf} should be avoided because it is dependent on cutoff parameters, not transferable to other simulation systems, and because using $\epsilon_{rf} = \infty$ yields considerably less disturbance of the dipole−dipole correlation. As it was shown before that one needs a cutoff of 4.0 nm before reaction field methods yield the same results as Ewald summation,[12] it is questionable whether reaction fields should be used at all.

3.4. Explanation for Layer Formation. Yonetani proposed[1] that the layering effect is in fact due to the cutoff, rather than due to the periodic boundary conditions. To prove this, he used simulations cells that were at most twice the volume of the original. In Figure 6 we have plotted again the $G_k(r)$ and $\langle\cos\rangle$ for cells 8 respectively 27 times the original cell, simulated with a cutoff. In addition, the 8-fold cell was simulated with PME. The size-dependence on $\langle\cos\rangle$ is very small, both when using a cutoff and when using PME, indicating that the relative orientation of the water molecules is not influenced by the size of the system or the periodic boundary conditions. Moreover, this shows that the particle-mesh Ewald method does not impose any artifacts on a water system of this size, which is the typical size for the solvation of a small protein. However, by a careful analysis of the dipole orientation parallel to the box axes (Figure 7) we find that there is a strong periodicity in the dipole along certain axes if the cutoff fits an integer number of times in the box. For a cutoff of 0.9 nm we find four periods in a box of roughly 4 nm, for a cutoff of 1.3 nm we find three periods, and for 1.8 nm we find 2 periods. However for a cutoff of 1.4 nm we find no obvious preference along the box axes, while it seems quite obvious that some orientational preference must exist. This can be explained if the layers are not parallel to the box axes but at an angle. In Figure 8 a schematic representation of such layer structures as observed in our simulations is given. Obviously, the layers are three-dimensional, but some "rules" can be inferred from the structures: the layers are equally thick and the layer thickness corresponds to roughly half the cutoff, or slightly more than so, and finally the number of layers must be even. In the case that the cutoff does not "fit" an integer times in the

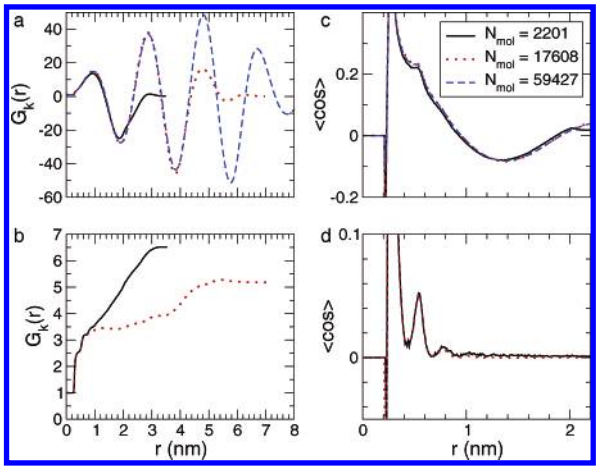

Figure 6. a: The $G_k(r)$ function as a function of system size for TIP3P water simulated with a cutoff of 1.8 nm, b: id. simulated with PME, c: $\langle\cos\rangle$ simulated with a cutoff of 1.8 nm, and d: id. simulated with PME.

Table 4. Simulation Results from Simulations of 2201 Molecules Using Two Water Models with a Reaction Field and Different ϵ_{rf}. Dielectric Constant $\epsilon(0)$ and Depth of Minimum in $G_k(r)$

SPC			SPC/E		
ϵ_{rf}	ϵ_0	G_k(min)	ϵ_{rf}	ϵ_0	G_k(min)
54.0	62(2)	1.19	62.3	67(3)	1.22
65.0	62(2)	1.24	77.0	73(3)	1.22
78.5	65(3)	1.44	78.5	77(4)	0.90
∞	64(4)	2.02	∞	72(4)	1.67

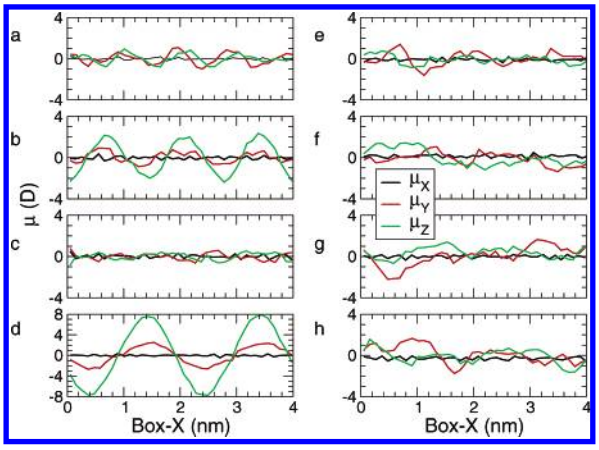

Figure 7. The components of the dipole moment summed over 40 slabs of roughly 0.1 nm along the *X*-axis of the box, for 2201 TIP3P molecules, simulated with different electrostatics treatment. a: Simulated with 0.9 nm cutoff, b: simulated with 1.3 nm cutoff, c: simulated with 1.4 nm cutoff, d: simulated with 1.8 nm cutoff (note different scale on the *Y*-axis), e: simulated with a reaction field with $\epsilon_{rf} = 78.5$ and a 1.8 nm cutoff, f: simulated with the particle-mesh Ewald technique with a cutoff of 0.9 nm, g: simulated with a switch function and a cutoff of 1.7 nm, and h: simulated with a shift function.

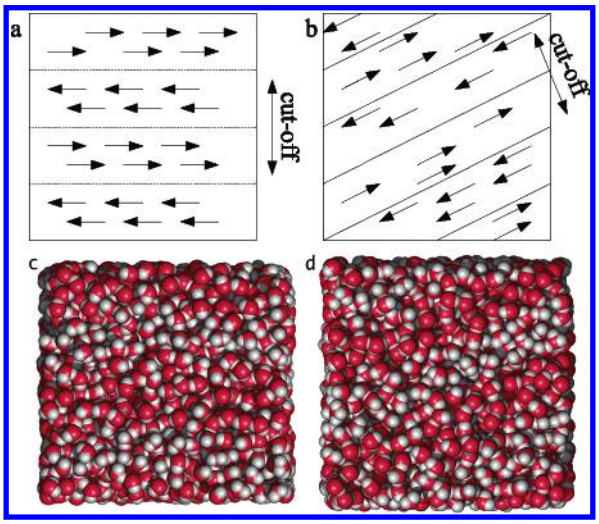

Figure 8. Schematic 2D picture of layer formation, a: four layers parallel to a box plane and b: four layers at an angle. The orientation of the dipoles in each layer as well as the relation between layer thickness and cutoff is indicated; the layers are somewhat thicker than half the cutoff. Snapshots of c: 2201 TIP3P molecules simulated with a cutoff of 1.8 nm (4 layers) and d: 2201 TIP3P molecules simulated with a cutoff of 1.5 nm (4 layers at an angle). Obviously when the box is cut at an angle the layers get thinner, to keep the same volume per slab.

box, the layers can form at an angle α given by

$$\cos \alpha = \frac{N(r_l)}{2l} \tag{3}$$

where N is the number of layers, r_l is the thickness of the layer, and l is the length of the box axis. In Figure 8d we estimate $\alpha \approx 25°$ yielding $r_l = 1.82$ nm, longer than the cutoff $r_c = 1.5$. For a similar snapshot (not shown) from the simulation with $r_c = 1.7$ nm, we find $\alpha \approx 14°$ yielding $r_l = 1.95$ nm. Apparently the layers can be 0.2−0.3 nm thicker than the cutoff. It is important to note that even with a moderate cutoff of 1.5, used in many simulations of biomolecules, significant layer formation takes place. In some cases (mainly in larger systems) we even observed multiple layer systems that existed simultaneously in the simulation, with the result that the value of ξ (eq 2) is low, making detection of layer formation problematic. The simulations performed with reaction field, PME, and switch and shift function do not display any regular pattern in the dipoles (Figure 7). The direct correlation between cutoff induced layer formation and periodic boundary conditions disagrees with Yonetani's conclusion that this is a pure cutoff effect.[1]

3.5. Other Systematic Tests. A number of other simple tests were performed in order to exclude systematic errors.

- A simulation using the Nosé-Hoover thermostat[46,47] and Parrinello-Rahman barostat[48] of 2201 TIP3P molecules with a 1.8 nm cutoff yielded identical $G_k(r)$ to the simulation using the Berendsen thermostat and barostat.[31] The diffusion constant in the Nose-Hoover simulation was larger (8.6 ± 0.2) than the one using Berendsen coupling (8.2 ± 0.8, Table 3) which could be due to systematic reduction of velocities by the Berendsen thermostat, although the difference is small and the error margin quite large.
- Simulations of 2201 TIP3P molecules were done with different pressure coupling constants τ_P in order to check its influence on layer formation and water mobility. For $\tau_P = 0$ (NVT simulation), 0.2, 0.5, and 2.0 ps no detectable difference in ξ (eq 2) could be found, and the $G_k(r)$ were very similar as well (not shown). The diffusion constants were 8.7 (NVT), 8.6 (0.2 ps), 8.2 (0.5 ps), and 8.8 10^5 cm^2 s^{-1} (2.0 ps), respectively. There is no clear trend that can be observed, and hence we conclude that τ_P is not relevant for layer formation.
- The TIP3P simulations using a group-based truncation with $r_c = 1.8$ nm and with the PME algorithm were continued to 10 ns. The $G_k(r)$ functions were virtually identical to those in the shorter simulations (data not shown). In combination with the finding that layer formation is reversible (Figure 3) this shows that our 2 ns simulations are long enough to justify our conclusions.
- All water models were simulated with an atom-based switch function and a switching range of 0.4 nm as well. Although the ripples that are present in Figure 4d have reduced amplitude with the longer switching range (not shown), they do not disappear altogether, implying that the atom-based switch function is not a viable solution for electrostatics treatment.[24] The observables in Table 3 lie between the 0.2 nm switching range and a shift function, as expected.
- A simulation of 2201 TIP3P molecules using double precision arithmetic (rather than the GROMACS default of single precision) yields identical $G_k(r)$ (not shown).

4. Discussion

In this work we have shown that an inappropriate use of simulation parameters can lead to artificial phase transitions.

TIP3P and TIP5P water and to some extent SPC/E and SPC as well were shown to form layers and change density abruptly (Figure 3b). The ordered layers are stabilized by a slightly larger number of hydrogen bonds (Figure 3f), leading to a lower potential energy. In addition, self-diffusion becomes anisotropic, and diffusion is considerably faster in the direction perpendicular to the layers (Figure 2). This artificial stabilization of the layered phase can be expected for all water models when simulated with group-based truncation of the potential; the extent to which it occurs varies between models as discussed below.

Figure 1 shows how the dipole−dipole correlation changes with increasing cutoff. It can be seen that there is a distinct minimum corresponding to anticorrelation (i.e. opposite dipoles[49]), which gets wider with increasing cutoff, while simultaneously the first, positive peak also gets wider. The turning point lies roughly at half the cutoff distance (0.6 nm for 1.2 nm cutoff, 0.84 for 1.5 nm, and 0.94 for 1.8 nm), and this turning point is unrelated to the real structure of water. This implies that for a given water molecule there is a large number of molecules with similar orientation until half the cutoff and an even larger number of molecules (due to the volume of the shell) with opposite orientation (Figure 8). The reason for this effect is that with a group-based cutoff, each water molecule is in effect at the center of a water cluster surrounded by vacuum, the free energy of one of these clusters is minimized by minimizing its net polarization, and hence the dipole moments become anticorrelated.[50] In combination with periodic boundary conditions this effect can lead to layer formation (Figure 7) which further strengthens the interaction. Figure 1c shows that the effect gets even more significant with longer cutoffs. Yonetani[1] suggested that the effect is entirely due to the cutoff; however, Figure 7 shows that some degree of ordering is always present when using a group-based cutoff, and it is particularly obvious when the box size is an (even) integer times the cutoff length. In extreme cases (Figure 3) periodic boundary conditions can enhance and stabilize the layers (Figure 8), in a similar fashion as an artificial wormlike periodic micelle was found to be induced by periodic boundary conditions.[51]

Mathias and Tavan have convincingly shown that there is no orientational correlation in water beyond 1.5 nm.[40] Our simulations with the particle mesh Ewald method[7,8] (Figure 4h) and with the shift function (Figure 4j) both agree with this observation. Although the shift function is well behaved in our simulations, it can obviously not be used for charged systems, while in simulations of neutral molecules the cutoff should be on the order of the real correlation length (for water 1.5 nm[40]). In addition, an ad-hoc addition of a shift function (in contrast to a switch) to a potential optimized without a shift function will change the relative energies in the potential at short distances (note that e.g. the ENCAD force field was calibrated for use with shifted potentials[43]). It seems therefore that a shift function is not an economic choice for neutral systems, while it is inappropriate for charged systems, despite being considerably more accurate than a cutoff.[52] A group-based switch function (Appendix B) could probably diminish the artifacts shown in Figure 4 and indeed be used without reparametrization of the force field, as the short-range interaction is unmodified. Like the shift function it cannot faithfully simulate ionic interactions. Finally, we have shown here that, at least for systems of 4 nm and larger, the PME method does not influence the orientational correlation (Figure 6) which confirms the findings of Mathias and Tavan.[40]

A question that remains is that of the difference between the water models. It has been shown that a large quadrupole can effectively quench the interactions between dipoles, leading to a reduced dielectric constant.[53−55] This is apparently what happens here: TIP4P has the largest quadrupole of the models tested (and the lowest dielectric constant) and is the least affected by the cutoff problems. In this context one could conclude that TIP4P is the most robust of the models used here. Even though e.g. the density maximum of water cannot be reproduced with TIP4P,[56] while that is possible with TIP5P,[28] it seems that the quadrupole of TIP4P is more realistic (note though, that the TIP4P variant that was optimized for use with Ewald summations, TIP4P-Ew[45] does have a density maximum close to the experimental one). Of the empirical models tested here, TIP4P is the only one with a realistic dimer structure,[57] even though the O−O distance is too short due to the effective charges. In addition, the latest versions of the OPLS force field[58] have been tuned for use with the TIP4P model, and simulations of proteins with the OPLS force field and TIP4P water are now beginning to appear.[59,60]

The question whether there is predictive value in water simulations[61] remains intriguing. Although Brodsky answered his own question with a clear no,[61] Guillot has taken a more constructive position, when comparing water models in a review recently.[62] It is somehow ironic that modeling a real phase transition, like freezing[20] takes enormous amounts of computer time, because it is a rare process, while artificial phase transitions such as the one reported here and by Yonetani[1] happen very fast. Van Gunsteren and Mark have published a series of criteria for the validation of molecular dynamics simulations.[27] An important criterion is that the quality of the result depends on the quality of the interaction function (including force field). From our results it is clear that only the particle-mesh Ewald[7,8] and the shift function yield a correct dipole−dipole correlation,[40] while in principle a group-based switch function should also give reliable results. Since neither a shift function nor a switch function can be used for charged systems, only methods that take the full Coulomb interaction into account remain as an option for biomolecular simulation.[26] A further method that we have not tested in this work is the Lekner summation[13,14] which is reported to give results that are in good agreement with experiments for liquid water[16] and which has been used for biomolecular simulation as well.[15]

Appendices

A. Coulomb Interaction with Reaction Field. The coulomb interaction can be modified for homogeneous systems, by assuming a constant dielectric environment beyond the cutoff r_c with a dielectric constant of ϵ_{rf}. The interaction then reads

$$V_{crf} = f\frac{q_i q_j}{r_{ij}}\left[1 + \frac{\epsilon_{rf} - 1}{2\epsilon_{rf} + 1}\frac{r_{ij}^3}{r_c^3}\right] - f\frac{q_i q_j}{r_c}\frac{3\epsilon_{rf}}{2\epsilon_{rf} + 1} \quad (4)$$

where $f = 1/(4\pi\epsilon_0)$ and ϵ_0 is the vacuum permittivity. The constant expression on the right makes the potential zero at the cutoff r_c. Note that at distances larger than r_c the potential *increases* which is relevant in the case of molecular based cutoffs.

B. Form of the Shift and Switch Functions. There is no fundamental difference between a shift function, which modifies a potential over its whole range ($0 \le r < r_c$), and a switch function, which modifies a potential over part of the range ($r_1 \le r < r_c$), since letting $r_1 = 0$ reduces a switch function to a shift function.[43] Switch or shift functions $S(r)$ can be applied to either the energy function $U(r)$ or the force function $F(r)$. In general a weighting function $W(r, r_1, r_c)$ is introduced:

$$W(r, r_1, r_c) = \begin{cases} 1 & \text{if } r < r_1 \\ \mathrm{S}(r,r_1,r_c) & \text{if } r_1 \le r < r_c \\ 0 & \text{if } r_c \le r \end{cases} \quad (5)$$

The switching function can be applied to atoms or to groups of atoms. In the latter case a definition of a group has to be made (e.g. the center of mass) and the value of the switching function is based on the distance R between group centers, and the value $S(R)$ is applied to all pairs of interactions.[24] Below we compare some switching functions $S(r)$ used in the literature to the one used in this work.

B.1. CHARMm Shift. In CHARMm[63] the Coulomb and Lennard Jones energy terms may be shifted ($r_1 = 0$) using

$$S(r, 0, r_c) = \left(1 - \left(\frac{r}{r_c}\right)^2\right)^2 \quad (6)$$

leading to, e.g., a shifted Coulomb force function

$$F_s(r, 0, r_c) = \frac{1}{r^2} + \frac{2}{r_c^2} - \frac{3r^2}{r_c^4} \quad (7)$$

which has a nonzero first derivative at the cutoff distance. This is, however, not a problem if the interactions are computed based on neutral groups.[43]

B.2. CHARMm Switch. A further option in CHARMm is to use a more involved switching function to the energy

$$S(r, r_1, r_c) = \frac{(r_c - r)^2(r_c + 2r - 3r_1)}{(r_c - r_1)^3} \quad (8)$$

this leads to the following Coulomb force function

$$F_s(r, r_1, r_c) = \frac{(r - r_c)(4r^2 + rr_c - 3r_1 r + r_c^2 - 3r_1 r_c)}{r^2(r_1 - r_c)^3} \quad (9)$$

This force has nonzero first derivatives at both r_1 and r_c. The authors of ref 64 mention problems with the robustness of the algorithms they used due to the discontinuities in the second derivative of eq 8.

B.3. ENCAD Shift. The shift function used for the ENCAD force field[43] is applied to the individual van der Waals energy and the Coulomb energy terms $U(r)$ according to

$$S(r, 0, r_c) = 1 - \frac{U(r_c)}{U(r)} - \frac{r - r_c}{U(r)}\frac{\partial U(r_c)}{\partial r} \quad (10)$$

for the Coulomb interaction this gives the following shift function

$$S(r, 0, r_c) = \left(1 - \left(\frac{r}{r_c}\right)\right)^2 \quad (11)$$

leading to a shifted Coulomb force function

$$F_s(r, 0, r_c) = \frac{1}{r^2} - \frac{1}{r_c^2} \quad (12)$$

which, like the CHARMm function, has a nonzero first derivative at the cutoff r_c.

B.4. OPLS Switch. Since the late 1980s OPLS force fields have been developed with a group-based switch function applied to the energy function (since the potentials are used for Monte Carlo no forces are used). The form is

$$S(r, r_1, r_c) = \frac{(r_c^2 - r^2)}{(r_c^2 - r_1^2)} \quad (13)$$

with r_1 typically $r_c - 0.05$ nm. This gives the following switched Coulomb force function:

$$F_s(r, r_1, r_c) = \frac{(r_c^2 - r^2)}{r^2(r_c^2 - r_1^2)} \quad (14)$$

The TIP5P model was developed with this switch function, but not the TIP3P and TIP4P models (W. L. Jorgensen, private communication), which, like SPC and SPC/E, were parametrized with group based truncation.

B.5. Ohmine Switch. A further switch function is used by Ohmine et al.[21,20] to multiply the energy with

$$S(r, r_1, r_c) = \frac{(r - r_c)^3[10(r - r_1)^2 - 5(r - r_1)(r - r_c) + (r - r_c)^2]}{(r_1 - r_c)^5} \quad (15)$$

in practice $r_1 = r_c - 0.2$ nm. This switch function results in a Coulomb force function that has no discontinuities in the first and second derivatives.

B.6. GROMACS Switch. The GROMACS switch[4−6] used in this work is applied to the force function $F(r)$ and is given by

$$S(r, r_1, r_c) = \frac{1 + A(r - r_1)^2 + B(r - r_1)^3}{r^{-(\alpha+1)}} \quad (16)$$

where α is the power of the interaction (1 for Coulomb, 6 and 12 for dispersion and repulsion, respectively). The constants A and B follow from the conditions that the function should be smooth at r_1 and r_c, hence

$$A = -\frac{(\alpha+4)r_c - (\alpha+1)r_1}{r_c^{\alpha+2}(r_c - r_1)^2}$$

$$B = \frac{(\alpha+3)r_c - (\alpha+1)r_1}{r_c^{\alpha+2}(r_c - r_1)^3} \quad (17)$$

Thus the total force function is

$$F_s(r, r_1, r_c) = \frac{1}{r^{\alpha+1}} + A(r - r_1)^2 + B(r - r_1)^3 \quad (18)$$

When $r_1 = 0$, the modified Coulomb force function is

$$F_s(r, r_1, r_c) = \frac{1}{r^2} - \frac{5r^2}{r_c^4} + \frac{4r^3}{r_c^5} \quad (19)$$

Like the Ohmine switch, this function has a smooth force at r_c and at r_1.

Supporting Information Available: Data corresponding to Figures 4 and 5 This material is available free of charge via the Internet at http://pubs.acs.org.

References

(1) Yonetani, Y. *Chem. Phys. Lett.* **2005**, *406*, 49−53.

(2) Jorgensen, W. L.; Chandrasekhar, J.; Madura, J. D.; Impey, R. W.; Klein, M. L. *J. Chem. Phys.* **1983**, *79*, 926−935.

(3) Pearlman, D. A.; Case, D. A.; Caldwell, J. W.; Ross, W. S.; Cheatham III, T. E.; DeBolt, S.; Ferguson, D.; Seibel, G.; Kollman, P. *Comput. Phys. Comm.* **1995**, *91*, 1−41.

(4) Berendsen, H. J. C.; van der Spoel, D.; van Drunen, R. *Comput. Phys. Comm.* **1995**, *91*, 43−56.

(5) Lindahl, E.; Hess, B. A.; van der Spoel, D. *J. Mol. Model* **2001**, *7*, 306−317.

(6) van der Spoel, D.; Lindahl, E.; Hess, B.; Groenhof, G.; Mark, A. E.; Berendsen, H. J. C. *J. Comput. Chem.* **2005**, *26*, 1701−1718.

(7) Darden, T.; York, D.; Pedersen, L. *J. Chem. Phys.* **1993**, *98*, 10089−10092.

(8) Essmann, U.; Perera, L.; Berkowitz, M. L.; Darden, T.; Lee, H.; Pedersen, L. G. *J. Chem. Phys.* **1995**, *103*, 8577−8592.

(9) Hockney, R. W.; Eastwood, J. W. *Computer simulation using particles;* McGraw-Hill: New York, 1981.

(10) Hünenberger, P. H. *J. Chem. Phys.* **2002**, *116*, 6880−6897.

(11) Greengard, L.; Rokhlin, V. *J. Comput. Phys.* **1987**, *73*, 325−348.

(12) Mathias, G.; Egwolf, B.; Nonella, M.; Tavan, P. *J. Chem. Phys.* **2003**, *118*, 10847−10860.

(13) Lekner, J. *Physica A* **1989**, *157*, 826−838.

(14) Lekner, J. *Physica A* **1991**, *176*, 485−498.

(15) Juffer, A. H.; Shepherd, C. M.; Vogel, H. J. *J. Chem. Phys.* **2001**, *114*, 1892−1905.

(16) English, N. J. *BTmph* **2005**, *103*, 1945−1960.

(17) van der Spoel, D.; van Maaren, P. J.; Berendsen, H. J. C. *J. Chem. Phys.* **1998**, *108*, 10220−10230.

(18) Slovák, J.; Tanaka, H. *BTjcp* **2005**, *122*, 204512.

(19) Zangi, R.; Mark, A. E. *Phys. Rev. Lett.* **2003**, *91*, 025502.

(20) Matsumoto, M.; Saito, S.; Ohmine, I. *Nature* **2002**, *416*, 409−413.

(21) Ohmine, I.; Tanaka, H.; Wolynes, P. G. *J. Chem. Phys.* **1988**, *89*, 5852−5860.

(22) Yamada, M.; Mossa, S.; Stanley, H. E.; Sciortino, F. *Phys. Rev. Lett.* **2002**, *88*, 195701.

(23) Allen, M. P.; Tildesley, D. J. *Computer Simulations of Liquids;* Oxford Science Publications: Oxford, 1987.

(24) Leach, A. R. *Molecular modelling: principles and applications;* Addison-Wesley Longman: Harlow, U.K., 1996.

(25) Koga, K.; Tanaka, H.; Zeng, X. C. *Nature* **2000**, *408*, 564−567.

(26) Hermans, J. *Proteins: Struct., Funct., Genet.* **1997**, *27*, i.

(27) van Gunsteren, W. F.; Mark, A. E. *J. Chem. Phys.* **1998**, *108*, 6109−6116.

(28) Mahoney, M. W.; Jorgensen, W. L. *J. Chem. Phys.* **2000**, *112*, 8910−8922.

(29) Berendsen, H. J. C.; Postma, J. P. M.; van Gunsteren, W. F.; Hermans, J. In *Intermolecular Forces*; Pullman, B., Ed.; D. Reidel Publishing Company: Dordrecht, 1981; pp 331−342.

(30) Berendsen, H. J. C.; Grigera, J. R.; Straatsma, T. P. *J. Phys. Chem.* **1987**, *91*, 6269−6271.

(31) Berendsen, H. J. C.; Postma, J. P. M.; DiNola, A.; Haak, J. R. *J. Chem. Phys.* **1984**, *81*, 3684−3690.

(32) Miyamoto, S.; Kollman, P. A. *J. Comput. Chem.* **1992**, *13*, 952−962.

(33) Harvey, S. C.; Tan, R. K. Z.; Cheatham, T. E. *J. Comput. Chem.* **1998**, *19*, 726−740.

(34) Watts, R. O. *Mol. Phys.* **1974**, *28*, 1069−1083.

(35) van Gunsteren, W. F.; Berendsen, H. J. C.; Rullmann, J. A. C. *Discuss. Faraday Soc.* **1978**, *66*, 58−70.

(36) Neumann, M.; Steinhauser, O. *Mol. Phys.* **1980**, *39*, 437−454.

(37) Neumann, M. *Mol. Phys.* **1983**, *50*, 841−858.

(38) Smith, P. E.; van Gunsteren, W. F. *J. Chem. Phys.* **1994**, *100*, 3169−3174.

(39) Chipot, C.; Milot, C.; Maigret, B.; Kollman, P. A. *J. Chem. Phys.* **1994**, *101*, 7953−7962.

(40) Mathias, G.; Tavan, P. *J. Chem. Phys.* **2004**, *120*, 4393−4403.

(41) Ludwig, R. *Angew. Chem., Int. Ed.* **2001**, *40*, 1808−1827.

(42) Buckingham, A. D. *Quart. Rev. (London)* **1959**, *13*, 183−214.

(43) Levitt, M.; Hirshberg, M.; Sharon, R.; Daggett, V. *Comput. Phys. Comm.* **1995**, *91*, 215−231.

(44) Wensink, E. J.; Hoffmann, A. C.; van Maaren, P. J.; van der Spoel, D. *J. Chem. Phys.* **2003**, *119*, 7308−7317.

(45) Horn, H. W.; Swope, W. C.; Pitera, J. W.; Madura, J. D.; Dick, T. J.; Hura, G. L.; Head-Gordon, T. *J. Chem. Phys.* **2004**, *120*, 9665−9678.

(46) Nosé, S. *Mol. Phys.* **1984**, *52*, 255−268.

(47) Hoover, W. G. *Phys. Rev. A* **1985**, *31*, 1695−1697.

(48) Parrinello, M.; Rahman, A. *J. Appl. Phys.* **1981**, *52*, 7182−7190.

(49) Hess, B. *J. Chem. Phys.* **2002**, *116*, 209−217.

(50) Straatsma, T. P.; Berendsen, H. J. C. *J. Chem. Phys.* **1988**, *89*, 5876−5886.

(51) Marrink, S. J.; Tieleman, D. P.; Mark, A. E. *J. Phys. Chem. B* **2000**, *104*, 12165−12173.

(52) Beck, D. A. C.; Armen, R. S.; Daggett, V. *Biochemistry* **2005**, *44*, 609−616.

(53) Carnie, S. L.; Patey, G. N. *Mol. Phys.* **1982**, *47*, 1129.

(54) Fries, P. H.; Richardi, J.; Krienke, H. *Mol. Phys.* **1997**, *90*, 841−854.

(55) Rick, S. W. *J. Chem. Phys.* **2004**, *120*, 6085−6093.

(56) Jorgensen, W. L.; Jenson, C. *J. Comput. Chem.* **1998**, *19*, 1179−1186.

(57) van Maaren, P. J.; van der Spoel, D. *J. Phys. Chem. B* **2001**, *105*, 2618−2626.

(58) Jorgensen, W. L. Wiley: New York, 1998; Vol. 3, chapter OPLS Force Fields, pp 1986−1989.

(59) van der Spoel, D.; Lindahl, E. *J. Phys. Chem. B* **2003**, *117*, 11178−11187.

(60) Seibert, M.; Patriksson, A.; Hess, B.; van der Spoel, D. **2005**, in press.

(61) Brodsky, A. *Chem. Phys. Lett.* **1996**, *261*, 563−568.

(62) Guillot, B. *J. Mol. Liq.* **2002**, *101*, 219−260.

(63) Brooks, B. R.; Bruccoleri, R. E.; Olafson, B. D.; States, D. J.; Swaminathan, S.; Karplus, M. *J. Comput. Chem.* **1983**, *4*, 187−217.

(64) Leslie, L. J.; Berne, B. J. *J. Phys. Chem. A* **1997**, *107*, 4350−4357.

(65) Hess, B.; Saint-Martin, H.; Berendsen, H. J. C. *J. Chem. Phys.* **2002**, *116*, 9602−9610.

(66) Jonas, J.; DeFries, T.; Wilbur, D. J. *J. Chem. Phys.* **1976**, *65*, 582−588.

(67) Price, W. S.; Ide, H.; Arata, Y. *J. Phys. Chem. A* **1999**, *103*, 448−450.

(68) Weast, R. C. *Handbook of Chemistry and Physics;* CRC Press: Cleveland, OH, 1977.

(69) Schmidt, E. *Properties of Water and Steam in SI-Units;* Springer-Verlag: Berlin, 1969.

(70) Postma, J. P. M. A Molecular Dynamics Study of Water, Ph.D. Thesis, University of Groningen, 1985.

CT0502256